

Gaussian wavepacket dynamics and quantum tunneling in asymmetric double-well systems

Hideo Hasegawa*

Department of Physics, Tokyo Gakugei University, Koganei, Tokyo 184-8501, Japan

(Dated: September 8, 2021)

Abstract

We have studied dynamical properties and quantum tunneling in asymmetric double-well (DW) systems, by solving Schrödinger equation with the use of two kinds of spectral methods for initially squeezed Gaussian wavepackets. Time dependences of wavefunction, averages of position and momentum, the auto-correlation function, an uncertainty product and the tunneling probability have been calculated. Our calculations have shown that (i) the tunneling probability is considerably reduced by a potential asymmetry ΔU , (ii) a resonant tunneling with $|\Delta U| \simeq \kappa \hbar \omega$ is realized for motion starting from upper minimum of asymmetric potential wells, but not for motion from lower minimum ($\kappa = 0, 1, 2, \dots$; ω : oscillator frequency at minima), (iii) the reduction of the tunneling probability by an asymmetry is less significant for the Gaussian wavepacket with narrower width, and (iv) the uncertainty product $\langle \delta x^2 \rangle \langle \delta p^2 \rangle$ in the resonant tunneling state is larger than that in the non-resonant tunneling state. The item (ii) is in contrast with the earlier study [Mugnai *et al.*, Phys. Rev. A **38** (1987) 2182] which showed the symmetric result for motion starting from upper and lower minima.

Keywords: asymmetric double-well potential, Gaussian wavepacket, quantum tunneling

PACS numbers: 03.65.-w, 05.30.-d

*hideohasegawa@goo.jp

I. INTRODUCTION

Double-well (DW) systems have been extensively studied in a wide range of fields including physics, chemistry and biology (for a recent review on DW systems, see Ref. [1]). Quantum tunneling is one of the most fascinating phenomena in DW systems [2]. Much experimental and theoretical studies have been made in tunneling of a quantum particle in DW systems. Quantum tunneling of a particle is possible from one-side well to the other-side well through classically forbidden region. Well-known old examples of DW systems include an inversion of ammonia molecule. In recent years, there has been an advance in the experimental study on macroscopic quantum tunneling such as Josephson junction and Bose-Einstein condensation in a double trap.

DW potential does not have to be symmetric and it may be asymmetric in general. In many experiments, the asymmetry of the DW potential can be changed by modifying external parameters. However, most theoretical studies have been made for symmetric DW systems, and asymmetric systems have received less theoretical attention than symmetric ones [3–8]. This is because solving an asymmetric DW system is more difficult than a symmetric one. Theoretical studies on asymmetric DW systems have been made based on various approximate methods like the WKB for simplified artificial DW potentials which are analytically tractable but not realistic [2]. By using such DW potentials, Weiner and Tse [3], and Nieto *et al.* [4] showed that although the tunneling probability is significantly reduced by the potential asymmetry, it is enhanced when the asymmetry meets the resonance condition. Mugai *et al.* [5] studied the fractal nature of the trajectory in asymmetric DW systems. By using WKB, Song [6] studied an asymmetric DW system where the difference of the potential minima is close of a multiple of $\hbar\omega$ (harmonic frequency in the wells). Rastelli [7] obtained a semi-classical formula for the tunneling amplitude in asymmetric DW systems with the use of WKB method. Conventional theories for DW systems have adopted the two-level approximation where the initial state in one-dimensional system is assumed to be given by $\Psi(x, 0) = [\Psi_0(x) - \Psi_1(x)]/\sqrt{2}$, $\Psi_\nu(x)$ denoting the ν th ($\nu = 0, 1$) eigenfunction. In order to discuss the tunneling probability in asymmetric DW systems, Cordes and Das [8] proposed a generalized two-level approximation: related discussion will be given in Sec. IV.

For a study on dynamics of wavepacket or tunneling in DW systems, it is necessary to solve the time-dependent Schrödinger equation subject to appropriate initial and boundary

conditions [9]. In the past when quantum mechanics was born, it was very difficult to numerically solve the time-dependent Schrödinger equation even for a simple potential except for a harmonic oscillator (HO) potential. One had to develop approximation methods applicable to simple tractable DW models although they are not necessarily realistic. In recent years, however, there has been significant development in computer and its software. It is now possible for us to solve the time-dependent Schrödinger equation with sufficient accuracy, by using convenient packages such as MATHEMATICA, MATLAB and Maple.

The purpose of the present study is to numerically study dynamics of Gaussian wavepackets and to examine the effect of the asymmetry on quantum tunneling in asymmetric DW systems. Quite recently it has been pointed out that a potential asymmetry of a DW system has significant effects on its specific heat [10]. We expect that it is the case also for dynamical properties of DW systems. We will solve the time-dependent Schrödinger equation by the spectral method for a given squeezed Gaussian wavepacket [11, 12], adopting the realistic quartic DW potential. In order to investigate the influence of the initial state on dynamical properties, we adopt two squeezed Gaussian wavepackets with different parameters.

The paper is organized as follows. In Sec. II, we will briefly mention the model and calculation method employed in our study [13]. In solving the time-dependent Schrödinger equation, we have adopted the two kinds of spectral method A [Eq. (16)] and spectral method B [Eq. (22)] with energy matrix elements evaluated for a finite size N_m ($= 30$). By using the spectral method A, we have calculated time-dependences of the magnitude of wavefunction, expectation values of position and momentum, the auto-correlation function, the uncertainty product and the tunneling probability, whose results are reported in Sec. III. In Sec. IV the tunneling probability is discussed with the use of the spectral method B. We discuss also wavepacket dynamics when the Gaussian wavepacket starts from near the top of the DW potential. Sec. V is devoted to our conclusion.

II. ADOPTED MODEL AND CALCULATION METHOD

A. Asymmetric double-well systems

We assume a quantum DW system whose Hamiltonian is given by

$$H = \frac{p^2}{2m} + U(x) = H_0 + V(x), \quad (1)$$

where

$$U(x) = C(x^2 - x_s^2)^2 - d\left(\frac{x^3}{3} - x_s^2 x\right), \quad \left(C = \frac{m\omega^2}{8x_s^2}\right) \quad (2)$$

$$H_0 = \frac{p^2}{2m} + U_0(x), \quad (3)$$

$$U_0(x) = \frac{m\omega^2 x^2}{2}, \quad (4)$$

$$V(x) = U(x) - U_0(x). \quad (5)$$

Here m , x and p express mass, position and momentum, respectively, of a particle, $U(x)$ denotes the DW potential with a degree of the asymmetry d , H_0 signifies the Hamiltonian for an HO potential $U_0(x)$ with the oscillator frequency ω , and $V(x)$ stands for a perturbing potential to H_0 . The asymmetric DW potential $U(x)$ has locally stable minima at $x = \pm x_s$ and an unstable maximum at $x_u = d(2x_s^2/m\omega^2)$ with

$$U(\pm x_s) = \pm \frac{2dx_s^3}{3}, \quad (6)$$

$$U(x_u) = \frac{m\omega^2 x_s^2}{8} + \frac{d^2 x_s^2}{m\omega^2} - \frac{2d^4 x_s^4}{3m^3 \omega^6}, \quad (7)$$

$$\Delta U = U(x_s) - U(-x_s) = \frac{4dx_s^3}{3}. \quad (8)$$

A prefactor of C ($= m\omega^2/8x_s^2$) in Eq. (2) is chosen such that the DW potential $U(x)$ for $d = 0.0$ has the same curvature at the minima as the HO potential $U_0(x)$: $U''(\pm x_s) = U''_0(0) = m\omega^2$ [10, 13]. The asymmetry parameter d is assumed to be given by

$$-d_c < d < d_c = \frac{m\omega^2}{2x_s}, \quad (9)$$

for which x_u locates at $-x_s < x_u < x_s$. In our model calculations, we have adopted parameters of $m = \omega = 1.0$ and $x_s = 2\sqrt{2}$ which yield $d_c = 0.1768$ and $U''(\pm x_s) = U''_0(0) = 1.0$ for $d = 0.0$. The DW potential given by Eq. (2) for typical values of $d = 0.0$ (solid curve), $d = -0.01$ (dashed curve) and $d = -0.033$ (chain curve) is plotted in Fig. 1(a).

For the HO Hamiltonian H_0 , eigenfunction E_{0n} and eigenvalue $\phi_n(x)$ are given by

$$\phi_n(x) = \frac{1}{\sqrt{2^n n!}} \left(\frac{m\omega}{\pi\hbar}\right)^{1/4} \exp\left(-\frac{m\omega x^2}{2\hbar}\right) H_n\left(\sqrt{\frac{m\omega}{\hbar}} x\right), \quad (10)$$

$$E_{0n} = \left(n + \frac{1}{2}\right) \hbar\omega \quad (n = 0, 1, 2, \dots), \quad (11)$$

where $H_n(x)$ stands for the Hermite polynomials.

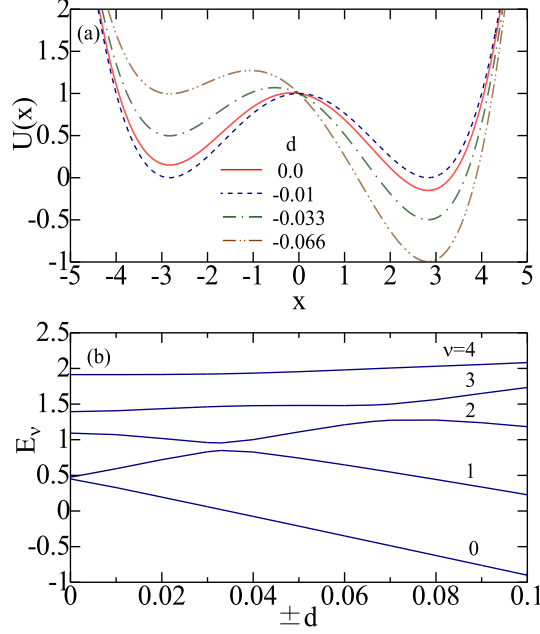


FIG. 1: (Color online) (a) The asymmetric DW potential for $d = 0.0$ (solid curve), $d = -0.01$ (dashed curve), $d = -0.033$ (chain curve) and $d = -0.066$ (double-chain curve) with $x_s = 2\sqrt{2}$ and $m = \omega = 1.0$ in Eq. (2). (b) Eigenvalues of E_ν ($\nu = 0$ to 4) as a function of $\pm d$. E_ν and $U(x)$ are symmetric and anti-symmetric, respectively, with respect to a sign of d .

For the stationary state, we solve the time-independent Schrödinger equation, expanding the eigenfunction $\Psi(x)$ in terms of $\phi_n(x)$

$$\Psi(x) = \sum_{n=0}^{N_m} c_n \phi_n(x), \quad (12)$$

leading to the secular equation

$$E c_n = \sum_{k=0}^{N_m} H_{nk} c_k, \quad (n = 0 \text{ to } N_m) \quad (13)$$

where E denotes the eigenvalue and N_m is the maximum quantum number. From a diagonalization of the secular equation, we obtain the eigenvalue E_ν and its relevant eigenfunction $\Psi_\nu(x)$ satisfying

$$H\Psi_\nu(x) = E_\nu\Psi_\nu(x). \quad (\nu = 0 \text{ to } N_m) \quad (14)$$

Figure 1(b) shows eigenvalues E_ν with $\hbar = 1.0$ for $\nu = 0 - 4$ as a function of $\pm d$. Table 1 shows $U(\pm x_s)$, $U(x_u)$, ΔU ($= U(x_s) - U(-x_s)$), δ ($= E_1 - E_0$) and δ' ($= E_2 - E_1$) as

a function of the asymmetry d . For $d > 0$ and $d < 0$, ΔU become $\Delta U > 0$ and $\Delta U < 0$, respectively. With increasing $|d|$, both $|\Delta U|$ and δ are increased. For $|d| \geq 0.02$, δ' becomes smaller than δ .

| d | $U(-x_s)$ | $U(x_u)$ | $U(x_s)$ | ΔU | δ | δ' |
|-------------|----------------|----------|----------------|----------------|----------|-----------|
| 0.0 | 0.0 | 1.0000 | 0.0 | 0.0 | 0.023923 | 0.61849 |
| ± 0.010 | ∓ 0.150849 | 1.0064 | ± 0.150849 | ± 0.301699 | 0.264823 | 0.47753 |
| ± 0.020 | ∓ 0.301699 | 1.02555 | ± 0.301699 | ± 0.603398 | 0.525453 | 0.29749 |
| ± 0.033 | ∓ 0.497803 | 1.06929 | ± 0.497803 | ± 0.995606 | 0.829368 | 0.10581 |
| ± 0.040 | ∓ 0.603398 | 1.10153 | ± 0.603398 | ± 1.2068 | 0.902893 | 0.17417 |
| ± 0.050 | ∓ 0.754247 | 1.15787 | ± 0.754247 | ± 1.50849 | 0.955426 | 0.36639 |
| ± 0.066 | ∓ 0.995606 | 1.27231 | ± 0.995606 | ± 1.99121 | 1.01905 | 0.66749 |

Table 1 Potential values at locally-stable minima ($\pm x_s$) and an unstable maximum position (x_u), $\Delta U [= U(x_s) - U(-x_s)]$, and energy gaps ($\delta = E_1 - E_0$, $\delta' = E_2 - E_1$) as a function of the asymmetry d for the asymmetric DW potential [Eq. (2)] ($N_m = 30$).

B. Spectral method A

For the non-stationary state, we solve the time-dependent Schrödinger equation given by

$$i\hbar \frac{\partial \Psi(x, t)}{\partial t} = H \Psi(x, t). \quad (15)$$

In the spectral method A, the eigenfunction $\Psi(x, t)$ is expanded in terms of $\phi_n(x)$

$$\Psi(x, t) = \sum_{n=0}^{N_m} c_n(t) \phi_n(x), \quad (16)$$

where $c_n(t)$ stands for the time-dependent expansion coefficient obeying equations of motion given by

$$i\hbar \frac{\partial c_n(t)}{\partial t} = \sum_{k=0}^{N_m} H_{nk} c_k(t) \quad (n = 0 \text{ to } N_m), \quad (17)$$

with

$$H_{nk} = E_{0n} \delta_{n,k} + \int_{-\infty}^{\infty} \phi_n(x)^* V(x) \phi_k(x) dx. \quad (18)$$

Equation (17) expresses the $(N_m + 1)$ first-order differential equations, which may be solved for a given initial condition of $\{c_n(0)\}$. An initial value of the expansion coefficient $c_n(0)$ is determined by

$$c_n(0) = \int_{-\infty}^{\infty} \phi_n(x)^* \Psi_G(x, 0) dx, \quad (19)$$

for the squeezed coherent Gaussian wavepacket $\Psi_G(x, 0)$ expressed by [11, 12]

$$\Psi_G(x, 0) = \frac{1}{(2\pi\mu)^{1/4}} \exp \left[-\frac{(1-i\alpha)}{4\mu}(x-x_0)^2 + i\frac{p_0(x-x_0)}{\hbar} \right], \quad (20)$$

where x_0 and p_0 are initial position and momentum, respectively, and parameters μ and α are related with

$$\langle \delta x^2 \rangle = \mu, \quad \langle \delta x \delta p + \delta p \delta x \rangle = \alpha. \quad (21)$$

C. Spectral method B

In an alternative spectral method B, the solution of the time-dependent Schrödinger equation given by Eq. (15) is expressed by

$$\Psi(x, t) = \sum_{\nu=0}^{N_m} a_{\nu} \Psi_{\nu}(x) e^{-iE_{\nu}t/\hbar}, \quad (22)$$

where $\Psi_{\nu}(x)$ and E_{ν} are eigenfunction and eigenvalue of the stationary state given by Eq. (14). Note that the expansion coefficient a_{ν} in Eq. (22) is time independent and it is determined by a given Gaussian wavepacket

$$a_{\nu} = \int_{-\infty}^{\infty} \Psi_{\nu}(x)^* \Psi_G(x, 0) dx. \quad (23)$$

Both spectral methods A and B yield the same result. Calculations of various time-dependent averages obtained by the spectral method A, which are presented in the Appendix, are easier than those by the spectral method B, while the latter method is physically more transparent than the former. By using mostly the spectral method A, we have performed model calculations to be reported in Sec. III. The spectral method B is employed for a discussion on the tunneling probability in Sec. IV. Wavefunctions obtained by the spectral methods have been cross-checked by the MATHEMATICA resolver for the partial differential equation.

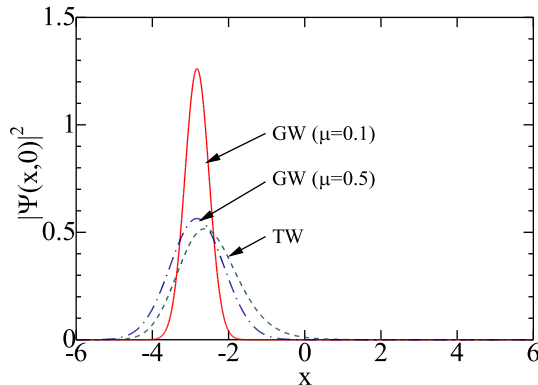


FIG. 2: (Color online) Magnitudes of Gaussian wavepackets (GWs) with $\mu = 0.1$ (solid curve) and $\mu = 0.5$ (chain curve), dashed curve showing the two-level wavepacket (TW): $\Psi(x, 0) = [\Psi_0(x) - \Psi_1(x)]/\sqrt{2}$.

III. MODEL CALCULATIONS

By using the method described in the preceding section, we have studied dynamics of Gaussian wavepackets in DW systems. Matrix elements H_{nk} in Eq. (18) for the adopted DW potential are given by Eq. (A5) in the Appendix. Model calculations for symmetric and asymmetric cases will be separately reported in Secs. III A and III B, respectively.

A. Symmetric case

First we consider the case of the symmetric potential with $d = 0.0$. A diagonalization of the energy matrix with $N_m = 30$ leads to eigenvalues of $E_\nu = 0.450203, 0.474126, 1.09262, 1.39334$ and 1.91286 for $\nu = 0$ to 4 , respectively, which are plotted in Fig. 1(b). The ground and first-excited states are quasi-degenerate with a energy gap of $\delta = 0.023923$. In order to examine effects of the Gaussian wavepacket on dynamical properties, we consider the two Gaussian wavepackets given by Eq. (20) with $\mu = 0.1$ and $\mu = 0.5$ for $x_0 = -x_s, p_0 = 0.0$ and $\alpha = 0.0$, which are plotted by solid and chain curves, respectively, in Fig. 2. The dashed curve will be explained later (Sec. IV).

Figures 3(a) and 3(b) show 3D plots of $|\Psi(x, t)|^2$ calculated by Gaussian wavepackets

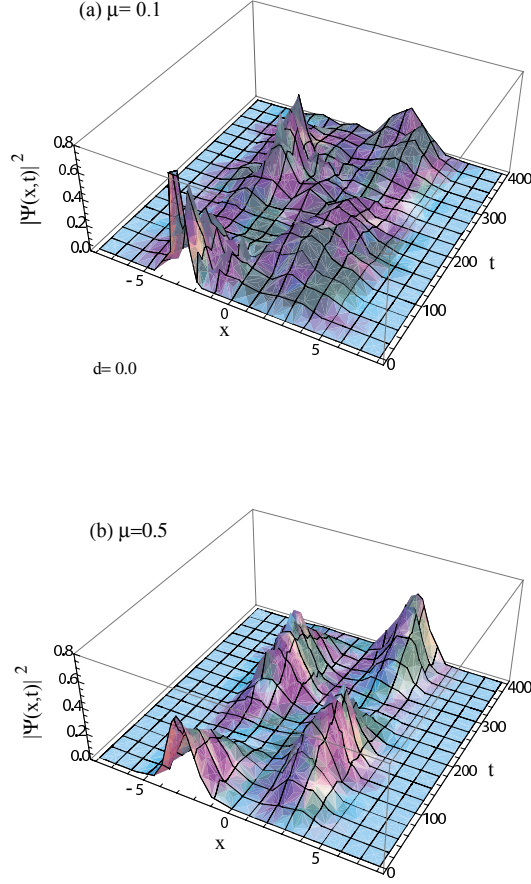


FIG. 3: (Color online) 3D plots of $|\Psi(x,t)|^2$ as functions of x and t for Gaussian wavepackets with (a) $\mu = 0.1$ and (b) $\mu = 0.5$ in the symmetric DW system ($x_0 = -2\sqrt{2}$, $p_0 = 0.0$).

with $\mu = 0.1$ and $\mu = 0.5$, respectively. As time is developing, initial Gaussian wavepackets are deformed, and wavepackets at $t > 0$ cannot be expressed by a single Gaussian [13].

Figures 4(a) and 4(b) show the auto-correlation function $|C(t)|^2$ for the Gaussian wavepackets with $\mu = 0.1$ and $\mu = 0.5$, respectively. Both auto-correlation functions oscillate with a period of about 260, which is consistent with the period given by $T = 2\pi/\delta = 262$.

Figures 5(a) and 5(b) show expectation values of $\langle x \rangle$ for Gaussian wavepackets with $\mu = 0.1$ and $\mu = 0.5$, respectively. It is clearly seen that a particle tunnels between the left and right wells with a period of about 260.

Figures 6(a) and 6(b) show the uncertainty product, $\langle \delta x^2 \rangle \langle \delta p^2 \rangle$, for Gaussian wavepackets with $\mu = 0.1$ and $\mu = 0.5$, respectively, where $\delta x = x - \langle x \rangle$ and $\delta p = p - \langle p \rangle$. They start from the minimum uncertainty of $\hbar^2/4$ at $t = 0$ and oscillate with fairly large magnitudes and with a period of about 130, a half of the period of $\langle x \rangle$ in Fig. 5. Its magnitude for

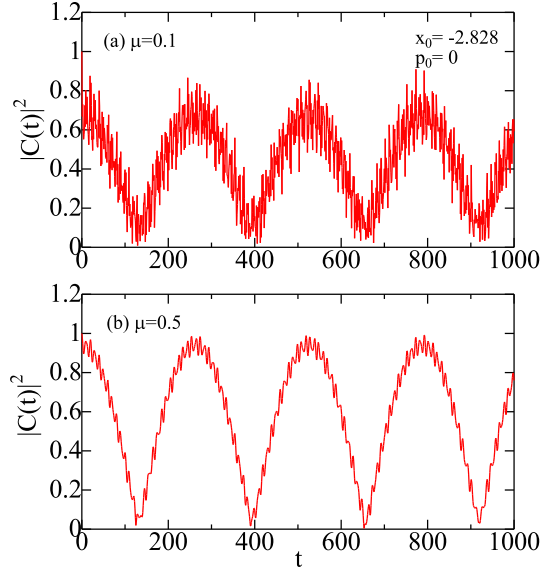


FIG. 4: (Color online) The time dependence of the auto-correlation function $|C(t)|^2$ in the symmetric DW system calculated for Gaussian wavepackets with (a) $\mu = 0.1$ and (b) $\mu = 0.5$ ($x_0 = -2\sqrt{2}, p_0 = 0.0$).

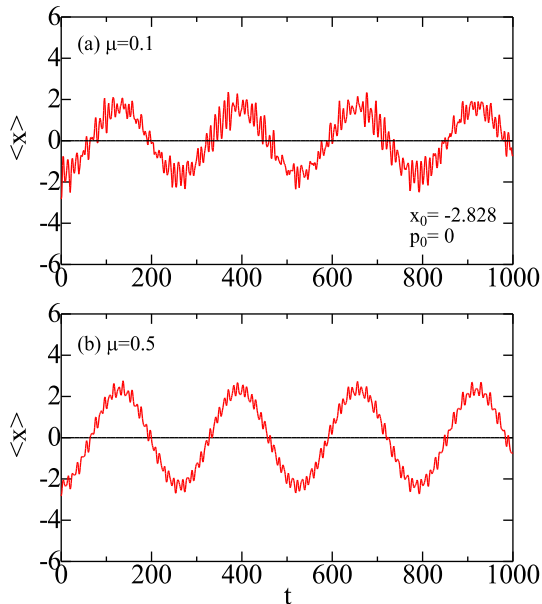


FIG. 5: (Color online) The time dependence of $\langle x \rangle$ in the symmetric DW system calculated for Gaussian wavepackets with (a) $\mu = 0.1$ and (b) $\mu = 0.5$ ($x_0 = -2\sqrt{2}, p_0 = 0.0$).

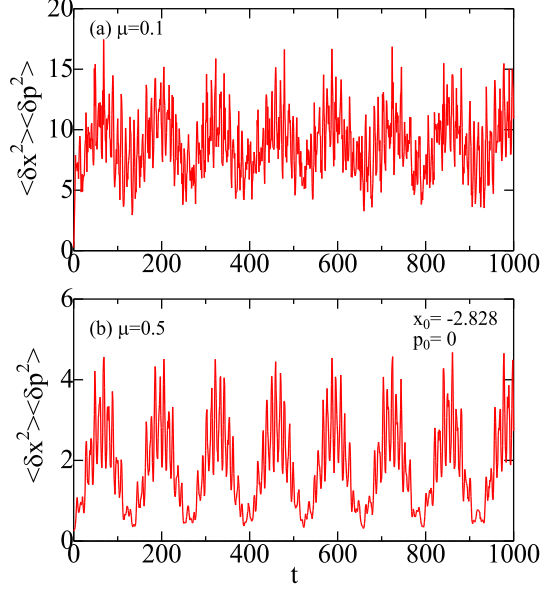


FIG. 6: (Color online) The time dependence of the uncertainty product: $\langle \delta x^2 \rangle \langle \delta p^2 \rangle$ in the symmetric DW system calculated for Gaussian wavepackets with (a) $\mu = 0.1$ and (b) $\mu = 0.5$ ($x_0 = -2\sqrt{2}, p_0 = 0.0$).

$\mu = 0.1$ is larger than that for $\mu = 0.5$ by a factor of about four.

B. Asymmetric case

Next we consider the asymmetric case with $d \neq 0$. For $d = -0.01$, the potential minimum in the right well is lower than that in the left well by $\Delta U = -0.301699$ (Table 1). We obtain eigenvalues of $E_\nu = 0.328786, 0.59361, 1.07114, 1.40643$ and 1.91312 for $\nu = 0 - 4$, respectively, which are plotted in Fig. 1(b). Quasi-degeneracy between E_0 and E_1 for $d = 0.0$ is removed by an introduced asymmetry, while E_2, E_3 and E_4 are almost independent of d .

Figures 7(a) and 7(b) show 3D plots of $|\Psi(x, t)|^2$ for $d = -0.01$ calculated by Gaussian wavepackets with $\mu = 0.1$ and $\mu = 0.5$, respectively, for $x_0 = -2\sqrt{2}, p_0 = 0.0$ and $\alpha = 0.0$. A comparison between Fig. 7(a) [Fig. 7(b)] and Fig. 3(a) [Fig. 3(b)] shows that $|\Psi(x, t)|^2$ for $d = -0.01$ stays in the left well and tunneling of a particle is almost vanishing. This is more clearly seen in Figs. 8(a) and 8(b) which show time dependences of $\langle x \rangle$ for $\mu = 0.1$ and $\mu = 0.5$, respectively..

We furthermore increase the asymmetry to $d = -0.033$, for which eigenvalues are $E_\nu =$

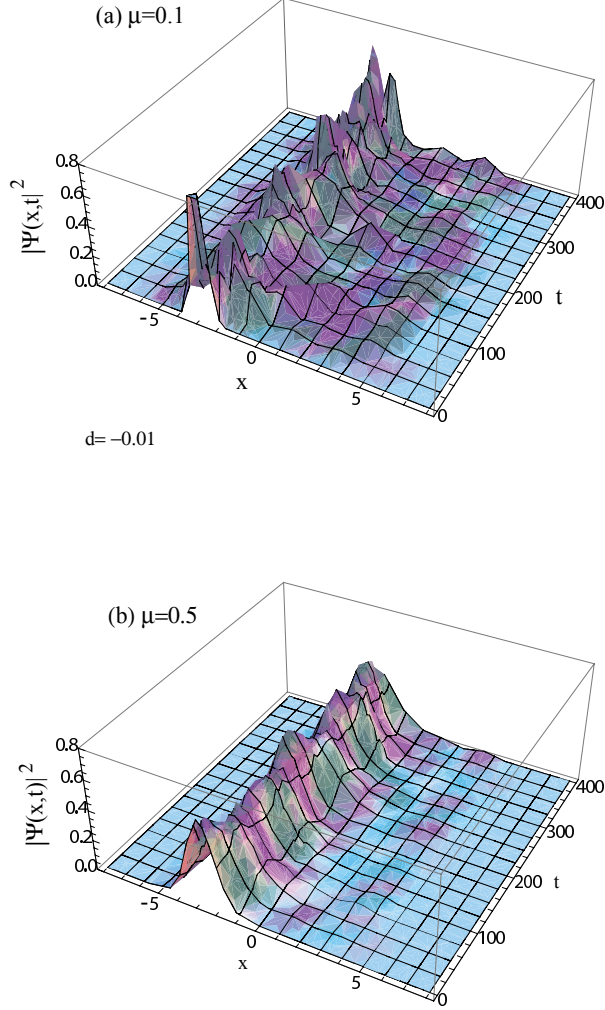


FIG. 7: (Color online) 3D plots of $|\Psi(x,t)|^2$ as functions of x and t calculated by Gaussian wavepackets with (a) $\mu = 0.1$ and (b) $\mu = 0.5$ in the asymmetric DW system with $d = -0.01$ ($x_0 = -2\sqrt{2}, p_0 = 0.0$).

0.0193182, 0.848686, 0.954496, 1.46802 and 1.92407, respectively [Fig. 1(b)]. The energy gap of δ ($= E_1 - E_0$) = 0.829368 is larger than δ' ($= E_2 - E_1$) = 0.10581, and the difference between two potential minima becomes $\Delta U = -0.995606$ (Table 1). We note that $\Delta U \simeq \omega = 1.0$, for which a resonance of tunneling is expected. Indeed, expectation values of $\langle x \rangle$ for $\mu = 0.1$ (Fig. 8(c)) and $\mu = 0.5$ (Fig. 8(d)) show tunneling with a period of about 60. This figure agrees with $2\pi/\delta' = 59.382$, which implies that contributions from the first- and second-excited states play important roles in the case of $d = -0.033$.

Figures 9(a)-9(d) show time dependences of the uncertainty product of $\langle \delta x^2 \rangle \langle \delta p^2 \rangle$ for

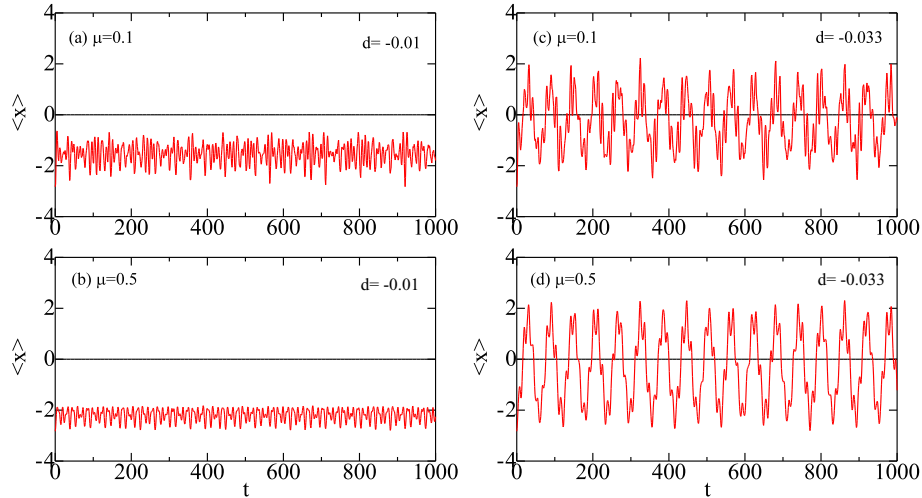


FIG. 8: (Color online) The time dependence of $\langle x \rangle$ in the asymmetric DW system calculated by Gaussian wavepackets with (a) $\mu = 0.1$ and (b) $\mu = 0.5$ for $d = -0.01$, and with (c) $\mu = 0.1$ and (d) $\mu = 0.5$ for $d = -0.033$.

$d = -0.01$ and -0.033 , which should be compared to those for $d = 0.0$ shown in Fig. 6. The uncertainty product for $d = -0.01$ is smaller than that for $d = 0.0$. It is, however, again increased for $d = -0.033$. We note that $\langle \delta x^2 \rangle \langle \delta p^2 \rangle$ in the resonant tunneling state with $d = 0.0$ or $d = -0.033$ is larger than that in the non-resonant tunneling state with $d = -0.01$. This is mainly due to the fact that $\langle \delta x^2 \rangle$ in the former state is larger than that in the latter. Magnitudes of uncertainty product for the Gaussian wavepacket with $\mu = 0.1$ are larger than that with $\mu = 0.5$.

The tunneling probability of $P_r(t)$ for finding a particle in the right well is defined by

$$P_r(t) = \int_0^\infty \Psi(x, t)^* \Psi(x, t) dx, \quad (24)$$

and its maximum by

$$P_r^{max} = \max_{\forall t} P_r(t). \quad (25)$$

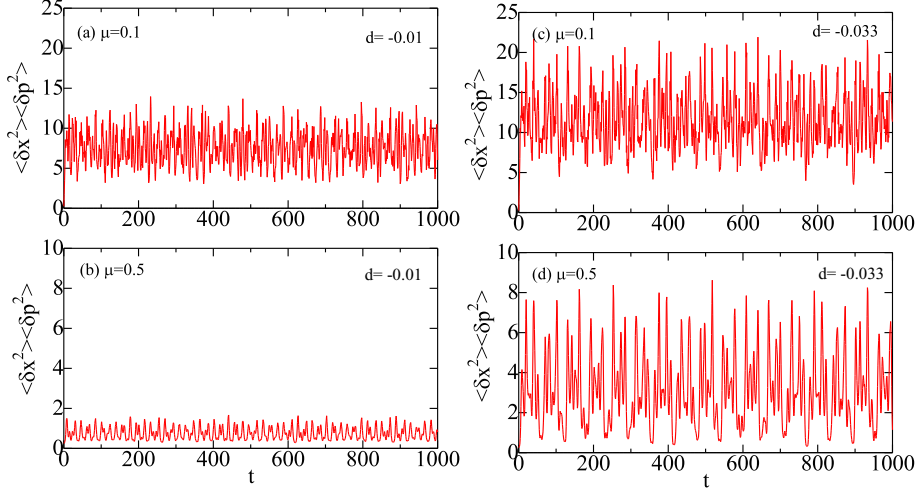


FIG. 9: (Color online) The time dependence of $\langle \delta x^2 \rangle \langle \delta p^2 \rangle$ in the asymmetric DW system calculated by Gaussian wavepackets with (a) $\mu = 0.1$ and (b) $\mu = 0.5$ for $d = -0.01$, and with (c) $\mu = 0.1$ and (d) $\mu = 0.5$ for $d = -0.033$.

Figures 10(a), 10(b) and 10(c) show $P_r(t)$ for $d = 0.0, -0.01$ and -0.033 , respectively, which are calculated by the Gaussian wavepacket with $\mu = 0.1$. For $d = 0.0$, $P_r(t)$ oscillates with a period of about 260, as shown in Figs. 4 and 5. For $d = -0.01$, $P_r(t)$ almost stay at about 0.2 where it significantly fluctuates. For $d = -0.033$, $P_r(t)$ again oscillates with a period of about 60, as shown in Figs. 8(c) and 8(d).

The maximum value of P_r^{max} is plotted as a function of ΔU in Fig. 11 where solid and dashed curves show the results calculated by Gaussian wavepackets with $\mu = 0.1$ and $\mu = 0.5$, respectively. The maximum value of $P_r^{max} \sim 1.0$ for symmetric DW case ($d = 0.0$) is considerably reduced by an introduced small asymmetry. For a negative $\Delta U = -0.995$ ($d = -0.033$), P_r^{max} shows an enhanced value due to a resonance effect, while there is no resonance for a positive $\Delta U = 0.995$ ($d = 0.033$). Similarly, the resonant tunneling is realized for a negative $\Delta U = -1.991$ ($d = -0.066$) but not for a positive $\Delta U = 1.991$ ($d = 0.066$).

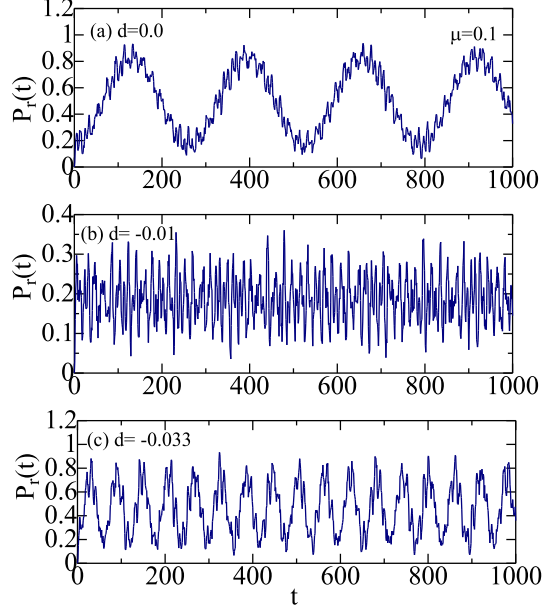


FIG. 10: (Color online) The time dependence of $P_r(t)$ in the asymmetric DW system with (a) $d = 0.0$, (b) $d = -0.01$ and (c) $d = -0.033$ calculated by the Gaussian wavepacket with $\mu = 0.1$.

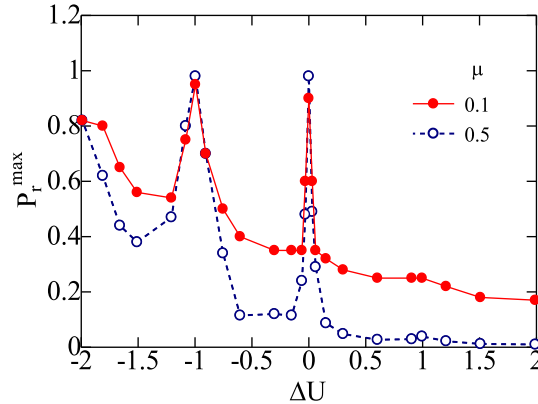


FIG. 11: (Color online) P_r^{max} as a function of ΔU calculated by Gaussian wavepackets with $\mu = 0.1$ (solid curve) and $\mu = 0.5$ (dashed curve).

The reduction of P_r^{max} by the asymmetry for the Gaussian wavepacket with $\mu = 0.5$ is more significant than that with $\mu = 0.1$. The ΔU dependence of P_r^{max} is not symmetric with respect to a sign of ΔU , which is in contrast with the result of Ref. [5].

IV. DISCUSSION

A. The potential-asymmetry dependence of P_r^{max}

We will discuss the d (or ΔU) dependence of the tunneling probability, by using the spectral method B presented in Sec. II B. From Eqs. (22) and (24), the tunneling probability is expressed by

$$P_r(t) = \sum_{\nu=0}^{N_m} \sum_{\lambda=0}^{N_m} a_\nu^* a_\lambda D_{\nu\lambda} e^{i\Delta E_{\nu\lambda} t/\hbar}, \quad (26)$$

with

$$D_{\nu\lambda} = \int_0^\infty \Psi_\nu(x)^* \Psi_\lambda(x) dx, \quad (27)$$

where $\Delta E_{\nu\lambda} = E_\nu - E_\lambda$. When main contributions arise from the two terms of $\nu = i$ and $\nu = j$ in Eq. (22), we may adopt the two-level approximation given by

$$\Psi(x, t) \simeq a_i \Psi_i(x) e^{-iE_i t/\hbar} + a_j \Psi_j(x) e^{-iE_j t/\hbar} \quad (a_i^2 + a_j^2 = 1), \quad (28)$$

leading to the tunneling probability

$$P_r(t) \simeq |a_i|^2 D_{ii} + |a_j|^2 D_{jj} + 2 \Re[a_i^* a_j D_{ij} e^{i\Delta E_{ij} t/\hbar}]. \quad (29)$$

Equations (23), (26) and (27) signify that $P_r(t)$ depends on the Gaussian wavepacket $\Psi_G(x, 0)$ and the asymmetry d through the d -dependent a_ν , E_ν and $\Psi_\nu(x)$.

Circles in Figs. 12(a) and 12(b) show magnitudes of calculated expansion coefficients $|a_\nu|^2$ of symmetric DW systems ($d = 0.0$) for Gaussian wavepackets with $\mu = 0.1$ and $\mu = 0.5$, respectively. The magnitude of $|a_\nu|^2$ for $\mu = 0.5$ in Fig. 12(b) has main contributions from $\nu = 0$ and $\nu = 1$, which is similar to the conventional two-level wavepacket: $\Psi(x, 0) = a_0 \Psi_0(x) + a_1 \Psi_1(x)$ with $|a_0|^2 = |a_1|^2 = 0.5$ plotted as the dashed curve in Fig. 2. In contrast, $|a_\nu|^2$ for $\mu = 0.1$ in Fig. 12(a) has extra contributions from $\nu = 5 - 7$ besides those from $\nu = 0$ and $\nu = 1$ although magnitudes of the former are smaller than those of the latter. From Eq. (29) the transition probability for $d = 0.0$ ($\Delta U = 0.0$) is given by

$$P_r(t) \simeq a_0^2 D_{00} + a_1^2 D_{11} + 2a_0 a_1 D_{01} \cos(\Delta E_{01} t/\hbar) \quad \text{for } \Delta U = 0.0. \quad (30)$$

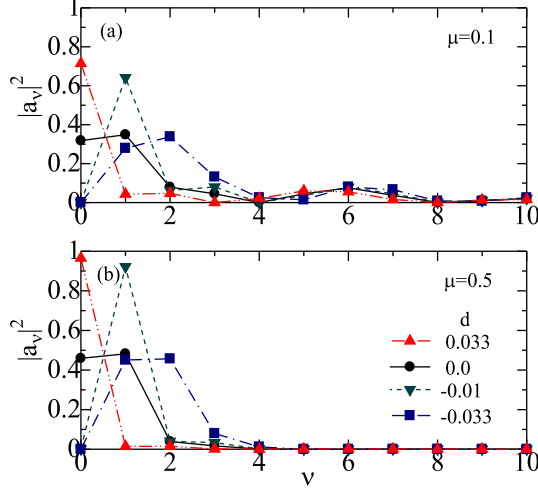


FIG. 12: (Color online) Magnitudes of expansion coefficients $|a_\nu|^2$ [Eq. (22)] against ν with $d = 0.033$ (triangles), $d = 0$ (circles), $d = -0.01$ (inverted triangles) and $d = -0.033$ (squares) for Gaussian wavepackets with (a) $\mu = 0.1$ and (b) $\mu = 0.5$.

Although Eq. (30) leads to a sinusoidal oscillation, $P_r(t)$ in Fig. 10(a) includes fine structures, which arise from high-frequency contributions neglected in the two-level approximation in Eq. (28). The essential feature of $P_r(t)$ for $d = 0.0$ in Fig. 10(a) may be explained by Eq. (30) with $|\Delta E_{01}| = \delta = 0.023923$ which yields $T = 2\pi/\delta = 262$.

When an asymmetry of $d = -0.01$ ($\Delta U = -0.3016$) is introduced, the dominant contribution comes from $\nu = 1$ both for $\mu = 0.1$ and $\mu = 0.5$ as shown by inverted triangles in Figs. 12(a) and 12(b). This suggests that the wavefunction for $d = -0.01$ may be given by the one-level state which yields the time-independent tunneling probability given by

$$P_r(t) \simeq a_1^2 D_{11} \quad \text{for } \Delta U = -0.3016. \quad (31)$$

Our calculation of $P_r(t)$ for $\Delta U = -0.3016$ ($d = -0.01$) in Fig. 10(b) shows wiggles, which arise from high-energy contributions not taken into account in the one-level approximation.

When an asymmetry is increased to $d = -0.033$ ($\Delta U = -0.9956$), main contributions to $|a_\nu|^2$ come from $\nu = 1$ and $\nu = 2$, as shown by squares in Figs. 12(a) and 12(b). From Eq. (29), we obtain the tunneling probability

$$P_r(t) \simeq a_1^2 D_{11} + a_2^2 D_{22} + 2a_1a_2 D_{12} \cos(\Delta E_{12} t/\hbar) \quad \text{for } \Delta U = -0.9956. \quad (32)$$

Indeed, $P_r(t)$ for $d = -0.033$ in Fig. 10(c) oscillates with a period of about 60 which is

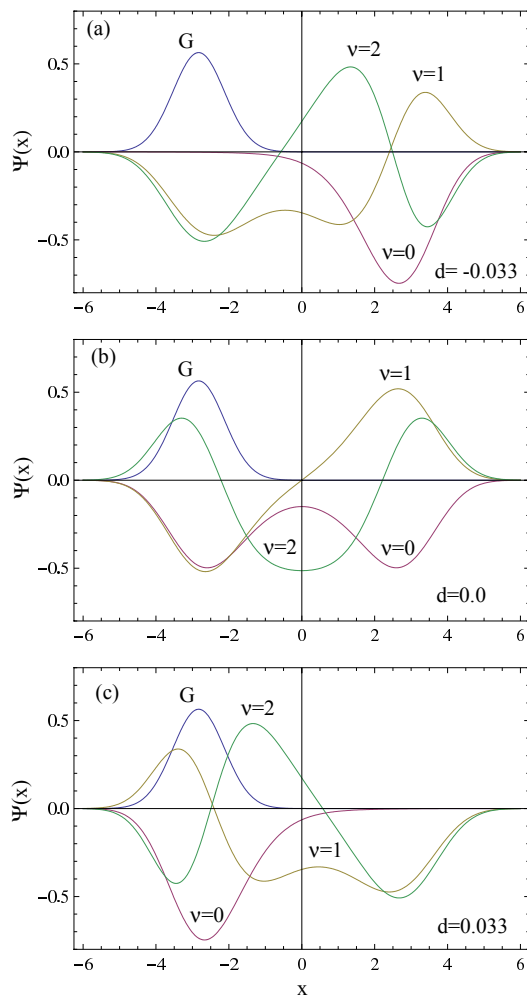


FIG. 13: (Color online) Gaussian wavepackets of $\Psi_G(x, 0)$ (G) with $\mu = 0.5$ and eigenfunctions of $\Psi_\nu(x)$ with $\nu = 0, 1$ and 2 for (a) $d = -0.033$, (b) $d = 0.0$ and (c) $d = 0.033$.

consistent with $T = 2\pi/\delta' = 59.382$ for $|\Delta E_{12}| = \delta' = 0.10581$ (Table 1).

For a negative ΔU , the $\nu = 0$ contribution to $|a_\nu|^2$ is completely suppressed as shown in Fig. 12. It is, however, not the case for a positive ΔU where the $\nu = 0$ contribution is predominant as shown by triangles for $d = 0.033$ ($\Delta U = 0.996$) in Fig. 12. The wavefunction is approximately expressed by the single $\nu = 0$ state which yields the time-independent tunneling probability

$$P_r(t) \simeq a_0^2 D_{00} \quad \text{for } \Delta U = 0.9956. \quad (33)$$

The result for a positive $\Delta U = 0.9956$ is in contrast to that for a negative $\Delta U = -0.9956$

given by Eq. (32).

In the following, we will elucidate the difference between the ν dependence of $|a_\nu|^2$ for $\Delta U = -0.9956$ and $\Delta U = 0.9956$, which may be understood from Eq. (23) expressed in terms of the eigenfunction of $\Psi_\nu(x)$ and the Gaussian wavepacket of $\Psi_G(x, 0)$. Eigenfunctions $\Psi_\nu(x)$ ($\nu = 0$ to 2) for the asymmetry of $d = -0.033$, $d = 0.0$ and $d = 0.033$ are plotted in Figs. 13(a), 13(b) and 13(c), respectively, where $\Psi_G(x, 0)$ with $\mu = 0.5$ is also shown. Figure 13(b) shows that the ground-state eigenfunction $\Psi_0(x)$ for $d = 0.0$ has the equal magnitude at $x = \pm x_s$. In contrast, $\Psi_0(x)$ for $d = -0.033$ at $x = x_s$ has a larger magnitude than that at $x = -x_s$ as shown in Fig. 13(a). On the other hand, Fig. 13(c) shows that the situation is reverse for $d = 0.033$: $|\Psi_0(-x_s)|^2 > |\Psi_0(x_s)|^2$. We note in Fig. 13(a) that magnitudes of a_1 and a_2 for $d = -0.033$ ($\Delta U = -0.9956$) may be appreciable because $\Psi_1(x)$ and $\Psi_2(x)$ overlap with $\Psi_G(x, 0)$. In contrast, Fig. 13(c) shows that a_1 and a_2 for $d = 0.033$ ($\Delta U = 0.9956$) become very small because $\Psi_1(x)$ and $\Psi_2(x)$ have nodes near the center of $\Psi_G(x, 0)$ while a_0 is appreciable because $\Psi_0(x)$ and $\Psi_G(x, 0)$ are overlap. It is necessary to note that high-energy contributions to $|a_\nu|^2$ at $\nu = 5 - 7$ for $\mu = 0.1$ are almost independent of the asymmetry in Fig. 12(a) while there are no such high-energy contributions for $\mu = 0.5$ in Fig. 12(b). This is the reason why the ΔU dependence of P_r^{max} for $\mu = 0.1$ is smaller than that for $\mu = 0.5$ as shown in Fig. 11.

When the asymmetry is much increased up to $d = \pm 0.066$ ($\Delta = \pm 1.991$), the energy gap between the second- and third-excited states: $E_3 - E_2 = 0.230984$ becomes smaller than δ and δ' with $E_2 (= 1.25498) \lesssim U(x_u) (= 1.27231) < E_3 (= 1.48597)$ [see Fig. 1 (b)]. Then for a negative $\Delta = -1.991$ ($d = -0.066$) dominant contributions to $|a_\nu|^2$ arise from two levels of $\nu = 2$ and $\nu = 3$, while for a positive $\Delta = 1.991$ ($d = 0.066$) a contribution from a single level of $\nu = 0$ is predominant (relevant results not shown). This is similar to the case of $\Delta U = -0.9956$ and $\Delta U = 0.9956$ mentioned above. We may similarly elucidate the difference between P_r^{max} of $\Delta U = -1.991$ and $\Delta U = 1.991$ in Fig. 11.

Cordes and Das (CD) [8] discussed the tunneling probability in asymmetric DW systems, proposing the generalized two-level wavefunction given by

$$\Psi^{CD}(x, t) = a_i \Psi_i^{CD}(x) e^{-iE_i t/\hbar} + a_j \Psi_j^{CD}(x) e^{-iE_j t/\hbar} \quad (a_i^2 + a_j^2 = 1). \quad (34)$$

Here eigenfunctions $\Psi_i^{CD}(x)$ and $\Psi_j^{CD}(x)$ of the DW system are assumed to be expressed by superposition of eigenfunctions for two harmonic potentials in left and right wells which

are separated by a high central barrier. By using Eq. (34), CD showed that the tunneling probability is given by [8]

$$P_r^{CD}(t) = 2a_i^2 a_j^2 [1 - \cos(\Delta E_{ij} t/\hbar)]. \quad (35)$$

The tunneling probability given by Eq. (35) is consistent with our results for $d = 0.0$ and $d = -0.033$ given by Eqs. (30) and (32), respectively. However Eq. (35) is not valid for cases of $d = -0.01$ and $d = 0.033$ for which it yields $P_r^{CD}(t) = 0$ in contrast to Eqs. (31) and (33). Actually, $P_r^{CD}(t)$ in Eq. (35) cannot be applied to the one-level state with either $a_i = 0$ or $a_j = 0$, while $P_r(t)$ given by Eq. (29) is applicable.

B. Varying initial Gaussian wavepacket

In our study reported in Secs. II and III, we have adopted the initial squeezed Gaussian wavepacket given by Eq. (20) with $x_0 = -2\sqrt{2}$, $p_0 = 0.0$, $\alpha = 0.0$ and $\mu = 0.1$ (or $\mu = 0.5$). We may, however, employ any arbitrary initial wavepacket with appropriate parameters of x_0 , p_0 , μ and α , while conventional theories rely on the two-level wavepacket. For example, we here employ an initial Gaussian wavepacket with $x_0 = 0.0$, $p_0 = 0.5$, $\mu = 0.1$ and $\alpha = 0.0$. In the classical mechanics, a particle with this initial condition rolls down from the origin near a top of the potential with an initial velocity of $v_0 = p_0/m = 0.5$, and it continues an oscillation at $-4 \lesssim x \lesssim 4$. Our calculation, however, shows that motion of a particle in quantum mechanics is quite different. The quantum average of x is given by $-0.5 \lesssim \langle x \rangle \lesssim 0.5$ for $d = 0.0$ and $-2 \lesssim \langle x \rangle \lesssim 2$ for $d = -0.033$ as shown in Figs. 14(a)-14(d). Quantum motion almost stays near the starting origin: it is difficult for a quantum particle to go across valleys located at $x = \pm 2\sqrt{2}$ [Fig. 1(a)]. The $\langle x \rangle$ vs. $\langle p \rangle$ plot in Figs. 14(a) and 14(b) shows that although classical paths are closed in the $\langle x \rangle$ - $\langle p \rangle$ space, quantum ones are not because of chaotic motion which is induced by quantum fluctuations as pointed out by Pattanayak and Schieve [14]. We note that results for the initial condition of $(x_0, p_0) = (0.0, 0.5)$ in Figs. 14(c) and 14(d) are quite different from relevant results for $(x_0, p_0) = (-2\sqrt{2}, 0.0)$ shown in Figs. 5(a) and 8(c). Thus the time dependence of $\langle x \rangle$ and other quantities depend on the assumed initial condition.

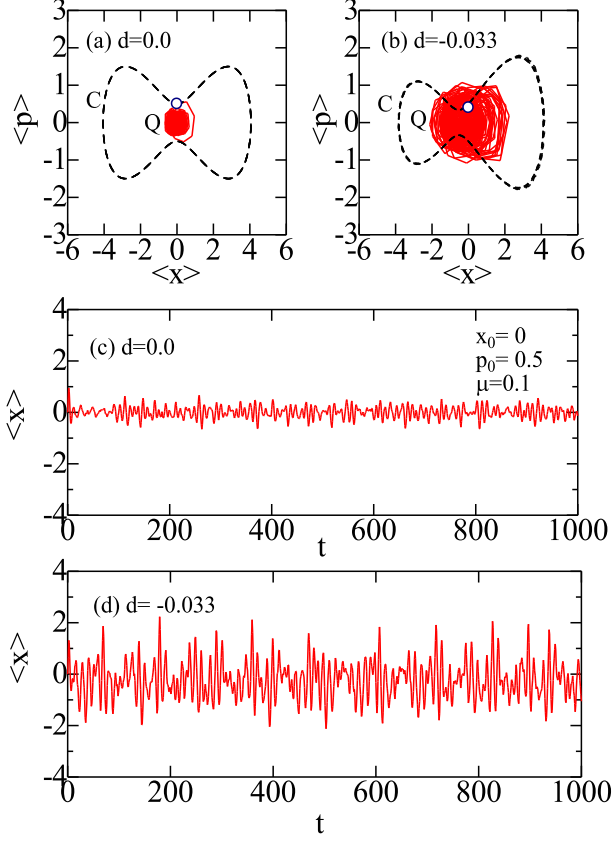


FIG. 14: (Color online) The $\langle x \rangle$ vs. $\langle p \rangle$ plot for (a) $d = 0.0$ and (b) $d = -0.033$ in the classical (C) (dashed curves) and quantum (Q) calculations (solid curves) with a time step of $\Delta t = 1.0$ for $t = 0.0 - 1000.0$ when a particle starts from the origin near the top of the DW potential, open circles denoting the starting point of $(x_0, p_0) = (0.0, 0.5)$. The time dependence of $\langle x \rangle$ for (c) $d = 0.0$ and (d) $d = -0.033$. Initial Gaussian wavepackets are given by Eq. (20) with $x_0 = 0.0$, $p_0 = 0.5$, $\mu = 0.1$ and $\alpha = 0.0$.

V. CONCLUSION

Dynamics of Gaussian wavepackets and quantum tunneling in asymmetric DW systems have been studied with the use of the numerical method which has advantages that (a) it is simple and physically transparent, (b) it is applicable to realistic DW potentials, and (c) it may adopt an arbitrary, appropriate initial state. Our calculations have shown the following:

- (1) The maximum tunneling probability P_r^{max} is considerably reduced by a small amount of the asymmetry ΔU in the DW potential,

(2) A resonant tunneling at $|\Delta U| \simeq \kappa \hbar \omega$ ($\kappa = 0, 1, \dots$) is not possible for motion starting from the lower minimum ($\Delta U > 0$) although it is possible for motion from upper minimum ($\Delta U < 0$) (Fig. 11),

(3) P_r^{max} for the Gaussian wavepacket with narrower width (μ) is less sensitive to the asymmetry, and

(4) The uncertainty product in the resonant tunneling state is larger than that in the non-resonant tunneling state.

The item (1) for $\Delta U \leq 0$ is consistent with results of previous studies [3, 4, 8]. The item (2) is against Ref. [5] which claimed the symmetric behavior for motion starting from the upper and lower minima. The item (3) is due to the fact that the Gaussian wavepacket with a small μ ($= 0.1$) includes high-energy contributions to a_ν whose magnitudes are nearly independent of the asymmetry (Fig. 12). The item (4) signifies that tunneling and uncertainty, both of which are typical quantum phenomena, are mutually related. In order to examine a validity of items (1)-(4), it would be interesting to observe $|\Psi(x, t)|^2$ in asymmetric DW systems, which seems difficult but possible with the recent advance of experimental methods. The present study has been made without considering dissipative effects which are expected to play important roles in stationary and dynamical properties of real DW systems. An inclusion of dissipation arising from environments is left as our future subject.

Acknowledgments

This work is partly supported by a Grant-in-Aid for Scientific Research from Ministry of Education, Culture, Sports, Science and Technology of Japan.

Appendix: Matrix elements and various expectation values

Matrix elements H_{nk} in Eq. (18) for the adopted DW potential are given as follows: We first rewrite $U(x)$ given by Eq. (2) as

$$U(x) = \frac{A_4 x^4}{4} + \frac{A_3 x^3}{3} + \frac{A_2 x^2}{2} + A_1 x + A_0, \quad (\text{A1})$$

with

$$A_4 = \frac{m\omega^2}{2x_s^2}, \quad A_3 = -d, \quad A_2 = -\frac{m\omega^2}{2}, \quad A_1 = d x_s^2, \quad A_0 = \frac{m\omega^2 x_s^2}{8}. \quad (\text{A2})$$

After some manipulations with the use of relations given by

$$q = \sqrt{\frac{g}{2}}(a^\dagger + a), \quad p = i\frac{\hbar}{\sqrt{2g}}(a^\dagger - a), \quad (g = \frac{\hbar}{m\omega}) \quad (\text{A3})$$

$$a^\dagger \phi_n = \sqrt{n+1} \phi_{n+1}, \quad a \phi_n = \sqrt{n} \phi_{n-1}, \quad (\text{A4})$$

we obtain the symmetric matrix elements H_{nk} for $n \geq k$ given by

$$\begin{aligned} H_{nk} = & \left[(n+1/2) \hbar\omega + \frac{3A_4g^2}{16}(2n^2 + 2n + 1) + \frac{A'_2g}{2}(n+1/2) + A_0 \right] \delta_{n,k} \\ & + \left[A_3 \left(\frac{g}{2}\right)^{3/2} n\sqrt{n} + A_1 \left(\frac{g}{2}\right)^{1/2} \sqrt{n} \right] \delta_{n-1,k} \\ & + \left[\frac{A_4g^2}{8}(n-1)\sqrt{n(n-1)} + \frac{A'_2g}{4}\sqrt{n(n-1)} \right] \delta_{n-2,k} \\ & + \frac{A_3}{3} \left(\frac{g}{2}\right)^{3/2} \sqrt{n(n-1)(n-2)} \delta_{n-3,k} \\ & + \frac{A_4g^2}{16} \sqrt{n(n-1)(n-2)(n-3)} \delta_{n-4,k}, \end{aligned} \quad (\text{A5})$$

where $A'_2 = A_2 - m\omega^2$ and $g (= \hbar/m\omega)$ is unity for $m = \omega = \hbar = 1.0$.

In the spectral method A, various time-dependent quantities may be expressed in terms of $\{c_n(t)\}$ as follows: After some manipulations with the use of the relations Eqs.(A3) and (A4), the auto-correlation function is given by

$$C(t) = \int_{-\infty}^{\infty} \Psi(x, t)^* \Psi(x, 0) dx, \quad (\text{A6})$$

$$= \sum_{n=0}^{N_m} c_n(t)^* c_n(0). \quad (\text{A7})$$

Expectation values of $x(t)$ and $p(t)$ are expressed by

$$\begin{aligned}\langle x(t) \rangle &= \int_{-\infty}^{\infty} \Psi^*(x, t) x \Psi(x, t) dx, \\ &= \sqrt{\frac{g}{2}} \sum_n \left[\sqrt{n+1} c_{n+1}^*(t) c_n(t) + \sqrt{n} c_{n-1}^*(t) c_n(t) \right],\end{aligned}\quad (\text{A8})$$

$$\langle p(t) \rangle = i \sqrt{\frac{\hbar^2}{2g}} \sum_n \left[\sqrt{n+1} c_{n+1}^*(t) c_n(t) - \sqrt{n} c_{n-1}^*(t) c_n(t) \right], \quad (\text{A9})$$

$$\begin{aligned}\langle x(t)^2 \rangle &= \left(\frac{g}{2}\right) \sum_n \left[\sqrt{(n+1)(n+2)} c_{n+2}^*(t) c_n(t) + (2n+1) c_n^*(t) c_n(t) \right. \\ &\quad \left. + \sqrt{n(n-1)} c_{n-2}^*(t) c_n(t) \right],\end{aligned}\quad (\text{A10})$$

$$\begin{aligned}\langle p(t)^2 \rangle &= - \left(\frac{\hbar^2}{2g}\right) \sum_n \left[\sqrt{(n+1)(n+2)} c_{n+2}^*(t) c_n(t) - (2n+1) c_n^*(t) c_n(t) \right. \\ &\quad \left. + \sqrt{n(n-1)} c_{n-2}^*(t) c_n(t) \right],\end{aligned}\quad (\text{A11})$$

$$\begin{aligned}\langle x(t)p(t) + p(t)x(t) \rangle &= i \hbar \sum_n \left[\sqrt{(n+1)(n+2)} c_{n+2}^*(t) c_n(t) \right. \\ &\quad \left. - \sqrt{n(n-1)} c_{n-2}^*(t) c_n(t) \right].\end{aligned}\quad (\text{A12})$$

On the contrary, in the spectral method B, calculations of time-dependent averages are more tedious than those in the spectral method A. For example, the expectation value of $x(t)$ is given by

$$\langle x(t) \rangle = \sum_{\nu} \sum_{\lambda} a_{\nu}^* a_{\lambda} X_{\nu\lambda} e^{i(E_{\nu} - E_{\lambda})t/\hbar}, \quad (\text{A13})$$

where

$$X_{\nu\lambda} = \int_{-\infty}^{\infty} \Psi_{\nu}(x)^* x \Psi_{\lambda}(x) dx. \quad (\text{A14})$$

-
- [1] M. Thorwart, M. Grifoni, and P. Hänggi, *Annals Phys.* **293**, 14 (2001).
[2] M. Razavy, *Quantum Theory of Tunneling* (World Scientific Publishing, Singapore 2003).
[3] J. H. Weiner and S. T. Tse, *J. Chem. Phys.* **74**, 2419 (1981).
[4] M. M. Nieto, V. P. Gutschick, C. M. Bender, F. Cooper and D. Strottman, *Phys. Lett. B* **163**, 336 (1985).
[5] D. Mugnai, A. Ranfagni, M. Montagna, O. Pilla, G. Viliani, and M. Cetica, *Phys. Rev. A* **38**, 2182 (1988).

- [6] Dae-Yup Song, *Annals. Phys.* **323**, 2991 (2008).
- [7] G. Rastelli, *Phys. Rev. A* **86**, 012106 (2012).
- [8] J. G. Cordes and A. K. Das, *Superlatt. Microstruct.* **29**, 121 (2001).
- [9] D. J. Tannor, *Introduction to quantum mechanics: A time-dependent perspective* (Univ. Sci. Books, Sausalito, California, 2007).
- [10] H. Hasegawa, *Phys. Rev. E* **86**, 061104 (2012).
- [11] F. Cooper, S.-Y. Pi, and P. N. Stancioff, *Phys. Rev. D* **34**, 3831 (1986).
- [12] Y. Tsue and Y. Fujiwara, *Prog. Theo. Phys.* **86**, 443 (1991).
- [13] H. Hasegawa, arXiv:1301.6423.
- [14] A. K. Pattanayak and W. C. Schieve, *Phys. Rev. Lett.* **72**, 2855 (1994).